The Retrieval of Ice Water Content from Radar Reflectivity Factor and Temperature and Its Use in Evaluating a Mesoscale Model

ROBIN J. HOGAN, MARION P. MITTERMAIER,* AND ANTHONY J. ILLINGWORTH

Department of Meteorology, University of Reading, Reading, United Kingdom

(Manuscript received 24 September 2004, in final form 11 June 2005)

ABSTRACT

Ice clouds are an important yet largely unvalidated component of weather forecasting and climate models, but radar offers the potential to provide the necessary data to evaluate them. First in this paper, coordinated aircraft in situ measurements and scans by a 3-GHz radar are presented, demonstrating that, for stratiform midlatitude ice clouds, radar reflectivity in the Rayleigh-scattering regime may be reliably calculated from aircraft size spectra if the "Brown and Francis" mass–size relationship is used. The comparisons spanned radar reflectivity values from −15 to +20 dBZ, ice water contents (IWCs) from 0.01 to 0.4 g m^{-3}, and median volumetric diameters between 0.2 and 3 mm. In mixed-phase conditions the agreement is much poorer because of the higher-density ice particles present. A large midlatitude aircraft dataset is then used to derive expressions that relate radar reflectivity and temperature to ice water content and visible extinction coefficient. The analysis is an advance over previous work in several ways: the retrievals vary smoothly with both input parameters, different relationships are derived for the common radar frequencies of 3, 35, and 94 GHz, and the problem of retrieving the long-term mean and the horizontal variance of ice cloud parameters is considered separately. It is shown that the dependence on temperature arises because of the temperature dependence of the number concentration "intercept parameter" rather than mean particle size. A comparison is presented of ice water content derived from scanning 3-GHz radar with the values held in the Met Office mesoscale forecast model, for eight precipitating cases spanning 39 h over southern England. It is found that the model predicted mean IWC to within 10% of the observations at temperatures between −30° and −10°C but tended to underestimate it by around a factor of 2 at colder temperatures.

1. Introduction

Ice clouds play an important role in the radiation budget of the earth (Liou 1986) and are the source of most surface precipitation globally, and so it is of major concern that the vertically integrated ice content simulated by the various climate models currently in use spans an order of magnitude (Stephens et al. 2002). Radar remote sensing from space offers the best hope of providing the necessary data to constrain the models, with the added advantage that the measurements would be at a high vertical resolution. Operational weather radars should also be capable of providing useful information on the denser ice clouds. Brown et al. (1995) estimated that spaceborne 94-GHz radar should be able to retrieve ice water content (IWC) to within a factor of 2 from radar reflectivity Z alone, with the error due to the fact that the radar measures a higher moment of the size distribution. However, they showed that if additional information was available on mean particle size (e.g., from the combination of radar and lidar) then the uncertainty could be reduced to around +40%/−30%. This remaining error is due to variations in the shape of the size distribution, including the possibility of bimodality.

Liu and Illingworth (2000) demonstrated that simple incorporation of temperature would make retrieved IWC significantly more accurate, exploiting the systematic changes in size distribution that occur with temperature. They also highlighted that the large differences between previously reported IWC–Z relationships (e.g., Liao and Sassen 1994; Atlas et al. 1995)

* Current affiliation: Met Office, Exeter, United Kingdom.

Corresponding author address: Robin J. Hogan, Department of Meteorology, University of Reading, Earley Gate, P.O. Box 243, Reading RG6 6BB, United Kingdom.
E-mail: r.j.hogan@reading.ac.uk

© 2006 American Meteorological Society

could be explained by the different radar frequencies considered and the wide range of assumptions on the relationship between particle mass and size. Using aircraft-measured ice size spectra they calculated best-fit relationships between Z and IWC in each 6°C temperature interval between −57° and −3°C. However, a problem arises in applying these to real cloud radar data in that discontinuities appear at the temperature boundaries every 6°C. Furthermore, application of the various relationships to the full range of observed radar reflectivity values and temperatures inevitably involves some of the relationships being applied outside the range of aircraft data from which they were derived, with a consequent increase in error and exacerbation of the problem of discontinuities.

In this paper, formulas that relate IWC to Z and temperature T are derived using the same aircraft data as were used by Liu and Illingworth (2000), but in such a way that retrieved IWC varies smoothly with both input parameters. Furthermore, a correction is performed for the known undercounting of small particles by the aircraft probes. Relationships are obtained for radar frequencies of 3 (i.e., Rayleigh scattering), 35, and 94 GHz, and, in addition to IWC, we also consider visible extinction coefficient α. These formulas represent the *expected value* of IWC or α for any given Z and T and would be suitable for comparison of instantaneous values or long-term averages with an independent estimate of the same parameter, such as the IWC held in a forecast model. However, because of the regression effect, the *variance* of retrieved IWC will tend to be underestimated by such relationships (Hogan and Illingworth 2003). Because cloud structure is of considerable importance for the radiative properties of ice clouds (Pomroy and Illingworth 2000; Fu et al. 2000; Carlin et al. 2002; Hogan and Kew 2005), we derive a parallel set of expressions to obtain the best estimate of the variance of IWC or α. These expressions would also yield the most accurate probability density functions (PDFs) of IWC and α.

The approach is then applied to 3-GHz scanning radar data to evaluate the IWC held in the Met Office mesoscale model during eight cases of frontal precipitation in southern England, spanning 39 h. The use of a relatively low frequency radar for studying ice clouds from the ground has the advantage over the more common use of radars at 35 and 94 GHz (e.g., Mace et al. 1997) that attenuation by intervening rain and melting ice is very low, enabling IWC to be retrieved in precipitating cases. Moreover, the fact that the particles scatter entirely in the Rayleigh regime makes the signals much easier to interpret.

In section 2 we show how IWC, α, and Z are obtained from data taken by the Met Office C-130 aircraft. The accuracy of aircraft-derived 3-GHz Z is evaluated in section 3 by comparison with coincident radar measurements. In section 4 we derive the relationship for IWC as a function of Z and T implicit in the assumptions of the Met Office model microphysics parameterization, and in section 5 a full set of relationships is derived from a large midlatitude dataset of C-130 ice-cloud observations from the European Cloud Radiation Experiment (EUCREX). The performance of the Met Office model is then evaluated in section 6.

2. Calculation of parameters from aircraft data

a. Theoretical background

The radar reflectivity factor of ice clouds is usually expressed assuming the particles to be spheres of diameter D consisting of a homogeneous mixture of ice and air with a density that varies with D alone (e.g., Brown et al. 1995):

$$Z = \frac{1}{0.93} \int_0^\infty n(D)|K(D)|^2 D^6 \gamma(D)\, dD, \qquad (1)$$

where $n(D)dD$ is the number concentration of particles with diameter between D and $D + dD$, $|K|^2$ is the dielectric factor (proportional to particle density squared), and γ is the Mie-to-Rayleigh backscatter ratio. In reality, ice particles are not spheres and a simple density relationship will not be strictly applicable to all of the particles in a radar sample volume, and so we generalize this formula to a summation over a volume V of particles of arbitrary habit:

$$Z = \frac{|K_i|^2}{0.93} \left(\frac{6}{\pi\rho_i}\right)^2 \frac{1}{V} \sum_j m_j^2 \gamma_j, \qquad (2)$$

where m_j is the mass of particle j, ρ_i is the density of solid ice and $|K_i|^2$ is the dielectric factor of solid ice (with the value 0.174 at all radar frequencies). The γ_j factor is now the ratio of the actual backscattering cross section to that predicted by Rayleigh theory and, in principle, could be calculated using a method other than Mie theory. In the Rayleigh-scattering limit it is more convenient to consider Z as simply proportional to mass squared as in (2) than to use (1) and to have to work with the concepts of "diameter" and "density," which are ill defined for arbitrarily shaped particles.

In the geometric optics approximation the visible extinction coefficient α is simply 2 times the integrated particle cross-sectional area A per unit volume. Thus, IWC and α may be expressed as summations over all particles in a volume V:

$$\mathrm{IWC} = \frac{1}{V}\sum_j m_j \quad \text{and} \tag{3}$$

$$\alpha = \frac{2}{V}\sum_j A_j. \tag{4}$$

b. The C-130 aircraft measurements

The EUCREX dataset used to derive the empirical relationships in section 5 is the same as that used by Brown et al. (1995), Liu and Illingworth (2000), and Hogan and Illingworth (2003), consisting of over 10 000 five-second-averaged size spectra measured by the Met Office aircraft in ice clouds around the United Kingdom in 1991 and 1992. We used a combination of the 2D cloud probe (2D-C), spanning the diameter range of 25–800 μm at 25-μm resolution, and the 2D precipitation probe (2D-P), spanning the diameter range of 200–6400 μm at 200-μm resolution. The same instruments were also used in the 1998 Cloud Lidar and Radar Experiment (CLARE'98) and the Clouds, Water Vapour, and Climate (CWVC) project, when radar was available for direct comparison (see section 3). Particle images intersecting the edge of the 2D-C or 2D-P photodiode array were excluded from the analysis, and the sample volume was reduced accordingly.

The 2D-C is known to undercount small particles (Heymsfield and Baumgardner 1985; Francis et al. 1998; Strapp et al. 2001), and so we modify the measured size distributions following Hogan and Illingworth (2003): the sub-100-μm particles are represented by a gamma distribution of solid-ice spheres that is constrained to have a modal diameter of 6 μm and to have the same concentration of 100-μm particles as measured by the 2D-C but 2 times as many of diameter 25 μm. This distribution increases the ice water content of the particles with diameter less than 90 μm by around a factor of 2.5, in agreement with the bias found by McFarquhar and Heymsfield (1997) when they compared a 2D-C with a video ice particle sampler. Although these authors used tropical rather than midlatitude data, we argue that the bias they found is instrumental in nature and thus should not vary significantly with geographical location. The effect of the correction on total IWC is fairly small, on average a 5% increase, but for α the effect is significantly greater at 29% and tends to increase for smaller values of α. Therefore, the error on retrievals of α using empirical relationships derived from the EUCREX dataset will have a significant contribution from the uncertainties in the small-particle correction. Note, however, that because of the dependence of radar reflectivity on a higher moment of the size distribution, the correction results in an average increase in 94-GHz Z of only 0.03 dB.

Some recent research (e.g., Gultepe et al. 2001; Boudala et al. 2002) has claimed that the forward-scattering spectrometer probe (FSSP) may provide a reasonable estimate of the number concentration of ice particles smaller than 50 μm, contrary to the original suggestion of Gardiner and Hallett (1985). This possibility implies that a larger small-particle correction than we have applied here may be necessary. However, it should be noted that the FSSP can be prone to overcounting because of particle shattering on collision with parts of the inlet of the probe (Field et al. 2003), and, even if the number concentration from the FSSP is accurate, the ice water content may be inaccurate because sizing of the particles requires knowledge of their shape. Furthermore, when Brown et al. (1995) included the FSSP data in their analysis of EUCREX data (assuming them to scatter like spheres) they found that in only 2.5% of observations did the FSSP contribute more than 50% of the total IWC, falling to 1.4% of cases when total IWC was greater than 10^{-3} g m^{-3}. Because the possibility of FSSP overcounting means that this is strictly an upper limit to the potential contribution of the sub-50-μm particles, we conclude that our approach of correcting the 2D-C by fitting a gamma distribution is reasonable.

The size spectra were available binned both by cross-sectional area A and the mean of the maximum dimensions measured parallel and perpendicular to the photodiode arrays D_m. Using this definition and a subset of the same EUCREX dataset (which included spectra with median volumetric diameters ranging from 0.15 to 1.3 mm), the following relationship was found by Brown and Francis (1995) to give the best agreement between the IWC inferred from the 2D probes and that from an independent evaporative technique:

$$\begin{aligned} m &= 0.0185 D_m^{1.9} \quad \text{for} \quad D_m \geq 9.7\times10^{-5}\,\mathrm{m} \quad \text{and} \\ &= 480 D_m^3 \quad \text{for} \quad D_m < 9.7\times10^{-5}\,\mathrm{m}, \end{aligned} \tag{5}$$

where m is in kilograms and D_m is in meters. This expression was originally proposed by Locatelli and Hobbs (1974) for "aggregates of unrimed bullets, columns and side-planes"; the use of simple power laws is widespread in the literature and in model parameterization schemes. Note that we use D_m rather than the (slightly larger) maximum particle dimension simply because it was used by Brown and Francis (1995); if we were to apply (5) to maximum particle dimension then we would systematically overestimate particle mass. Both IWC and Z were calculated from the D_m-binned data with particle mass m in (2) and (3) taken from (5). Extinction coefficient was calculated directly from the A-binned data using (4). The dependence of the re-

trievals on the assumed mass–size relationship is explored in section 4 and in the appendix.

For Rayleigh-scattering frequencies (e.g., 3 GHz) the factor γ in (2) is unity, implying that if we can make an unbiased estimate of m using (5) then Z calculated using (2) should also be unbiased. However, the fact that Z is proportional to mass squared means that it is more sensitive to the larger particles, for which (5) may be less accurate. In section 3 we show from coordinated aircraft flights and scans of a well-calibrated Rayleigh-scattering radar that (5) does indeed appear to be reliable for particle size well above 1 mm.

At higher frequencies (e.g., 35 and 94 GHz) the diameter of the larger particles may be an appreciable fraction of the radar wavelength, resulting in a decrease in the backscatter relative to that predicted by the Rayleigh approximation, that is, $\gamma < 1$. We follow the approach of numerous researchers and approximate the particles as homogeneous ice–air spheres and apply Mie theory to estimate γ. The question then arises as to what diameter to use for the sphere, assuming that the mass is still given by (5). Two possible candidates are D_m and the equivalent-area diameter D_a (i.e., the diameter of the sphere that has the same cross-sectional area A as the actual particle). This choice has a significant effect on calculated 94-GHz reflectivity, because D_m is typically 25% larger than D_a, which results in a lower value of γ when the particles are large.[1] Intuitively it might be expected that D_m should better represent the extremities of the particle, which are important when scattering departs from the Rayleigh approximation, although the recent results of Donovan et al. (2004) suggest that for idealized crystal shapes both D_a and D_m can be used to estimate Z to within 30%.

c. *A note on calibration*

The presence of the factor 0.93 (the dielectric factor of liquid water at centimeter wavelengths) in (1) and (2) ensures that in liquid clouds or rain at centimeter wavelengths the definition of radar reflectivity reduces to the familiar form

$$Z = \int_0^\infty n(D)D^6\, dD. \tag{6}$$

The fact that the dielectric factor of solid ice $|K_i|^2$ is independent of radar wavelength then means that all radars should measure the same value of Z in Rayleigh scattering ice cloud (but not liquid cloud), with this value referenced back to a centimeter-wavelength radar; this defines the calibration convention we have used. However, an alternative convention is that any radar operating in the centimeter- or millimeter-wavelength range should measure the Z given by (6) in Rayleigh-scattering liquid cloud at a particular reference temperature T_0. Care must then be taken because the dielectric factor of liquid water $|K_w|^2$ is both wavelength and temperature dependent; for a radar calibrated in this way, (1) changes to

$$Z = \frac{1}{|K_w(T_0)|^2}\int_0^\infty n(D)|K(D)|^2 D^6 \gamma(D)\, dD. \tag{7}$$

For $T_0 = 0°C$, $|K_w(T_0)|^2$ has the values 0.88 and 0.67 at 35 and 94 GHz, respectively. Hence, to apply the expressions derived in this paper to the data from such a radar, the measured Z would first have to be multiplied by $|K_w(T_0)|^2/0.93$, or, in conventional logarithmic units, 0.24 and 1.42 dB would have to be *subtracted* from the measured Z at 35 and 94 GHz, respectively.

At these higher frequencies a correction must also be made for attenuation by intervening atmospheric gases (particularly water vapor and molecular oxygen) calculated from an atmospheric sounding. Liquid water clouds and melting ice can also cause significant attenuation, but radar attenuation by ice clouds can generally be considered to be negligible up to 94 GHz (Hogan and Illingworth 1999).

3. Evaluation of aircraft estimates of radar reflectivity during CLARE'98 and CWVC

In this section we compare Z calculated from size spectra measured by the Met Office C-130 aircraft directly with the values measured by the Rayleigh scattering 3-GHz radar at Chilbolton, southern England, in five different cases. The data were taken during the CLARE'98 campaign (cases 1–3), which took place between 5 and 23 October 1998 in nonprecipitating clouds (European Space Agency 1999; Hogan et al. 2003), and two flights of the CWVC project (cases 4 and 5) in the autumn of 2000 (see Field et al. 2004). In each case the aircraft flew runs toward and away from Chilbolton along an azimuth close to 260° at around 100 m s^{-1}. The scanning 3-GHz radar at Chilbolton has a beamwidth of 0.28° and is calibrated to 0.5 dB using the technique of Goddard et al. (1994). The random error on data with a resolution of 300 m/0.25 s, averaged from four 75-m gates, is around 0.5 dB.

Figures 1–5 show cases 1–5, respectively, spanning temperatures from −31.9° to −6.9°C, reflectivity values

[1] Note that this issue is often phrased equivalently in terms of effective particle *density*, and that if a particle of a given mass is approximated by spheres with diameter differing by 25% then their effective density will differ by almost a factor of 2.

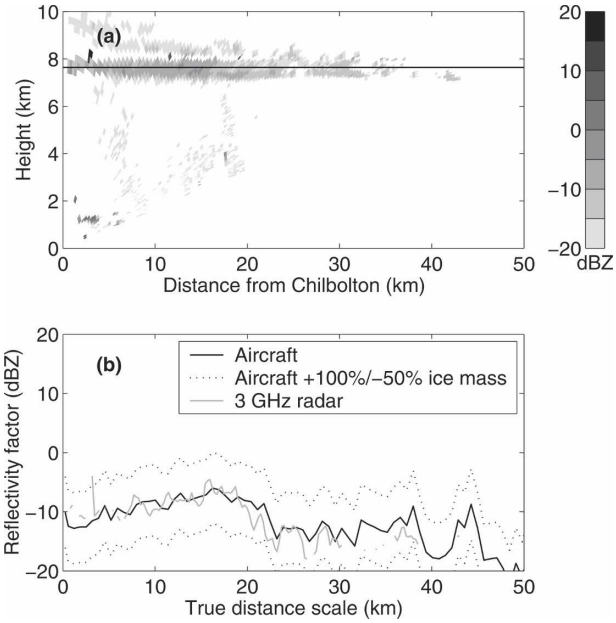

FIG. 1. (a) Reflectivity factor measured by the Chilbolton 3-GHz radar between 1430 and 1437 UTC 14 Oct 1998 with C-130 aircraft track at −31.9°C superimposed; (b) corresponding comparison of radar-measured and aircraft-derived reflectivity factor. The dotted lines lie 6 dB above and below the aircraft-derived Z, indicating the effect of an error in ice mass (or density) of a factor of 2 at all sizes.

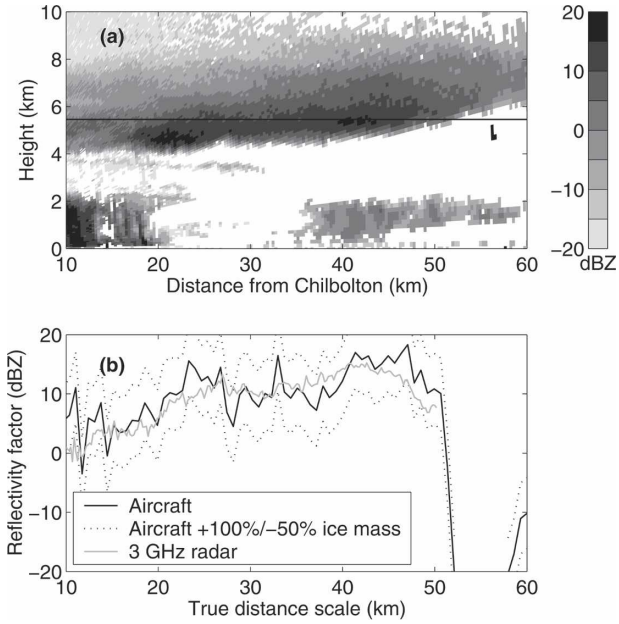

FIG. 2. As in Fig. 1, but between 1516 and 1521 UTC 20 Oct 1998, with the aircraft sampling at a temperature of −14.5°C.

from −15 to +20 dBZ, ice water contents of 0.01–0.4 g m^{-3} and median volumetric diameters of 0.2–3 mm. The results of the comparisons are summarized in Table 1. Where the samples were not simultaneous the aircraft data were shifted spatially using the measured wind component along the radar azimuth at the altitude of the sample. In accord with this procedure, the second panel of each of these figures is plotted using a "true" distance scale, whereby the wind speed at the height of the aircraft has been used to convert the finite-time sampling of both the radar and the aircraft into a distance scale equivalent to an instantaneous snapshot. The fact that Z is proportional to mass squared [see (2)] means that a factor-of-2 error in the assumed mass of all the particles in the aircraft analysis [i.e., varying a but not b in (10)] would result in approximately a factor-of-4 difference in the predicted Z; this is indicated in Figs. 1–5 as dashed lines 6 dB above and below the prediction using (5).

In Figs. 1 and 3, a slow but variable-speed vertical scan was performed to maximize collocation of the data by attempting to keep the C-130 in or close to the radar beam. The navigation data from the aircraft indicate that the aircraft and radar were coordinated very well in terms of distance from the radar but that at certain times in the run the aircraft was displaced laterally up to 500 m from the 260° azimuth used by the radar. However, cirrus variability is modest on scales smaller than 500 m [IWC varying by typically 15%–25% according to Hogan and Illingworth (2003)]. Indeed, in case 1 the agreement between radar and aircraft is good, with the aircraft calculating a reflectivity that is on average only 0.74 dB (i.e., 16%) more than that of the radar measurements. This result implies only an 8%

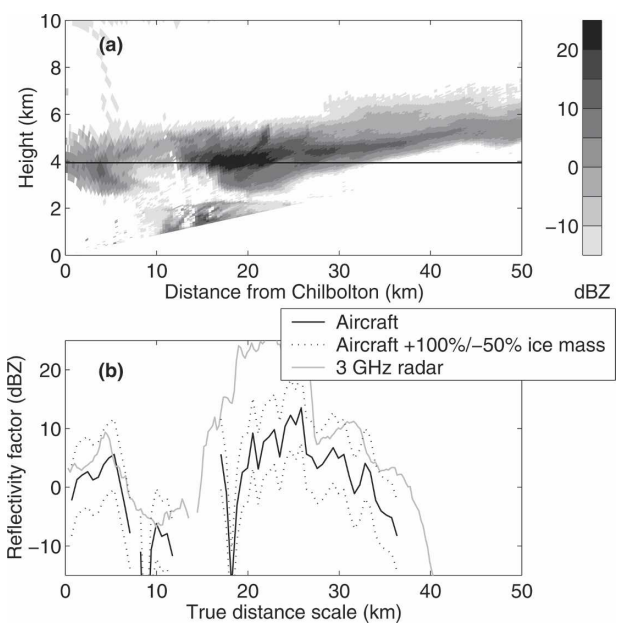

FIG. 3. As in Fig. 1, but between 1423 and 1433 UTC 20 Oct 1998, with the aircraft sampling at a temperature of −6.9°C.

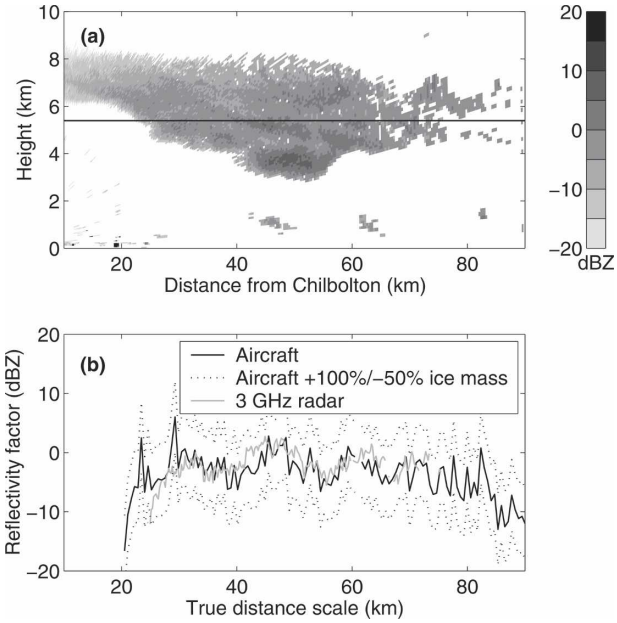

FIG. 4. As in Fig. 1, but between 1013 and 1027 UTC 20 Oct 2000, with the aircraft sampling at a temperature of −20.1°C.

error in the ice particle mass (and hence density) predicted by (5), justifying the use of a simple power law. The median volumetric diameter D_0 measured during this run was around 0.3 mm. The ±2-dB scatter in the comparison is likely to be a combination of the mismatch of the sample volumes, the reduced precision in the radar measurements at low signal-to-noise ratio,

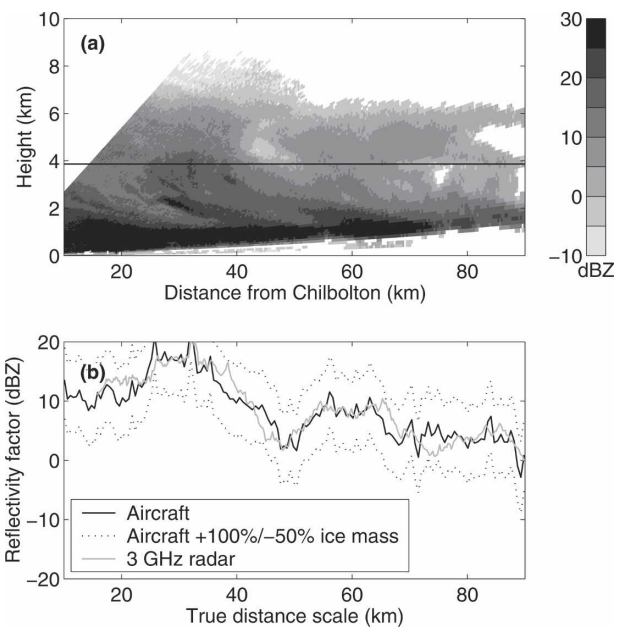

FIG. 5. As in Fig. 1, but between 1515 and 1527 UTC 21 Nov 2000, with the aircraft sampling at a temperature of −9.8°C.

TABLE 1. Summary of the comparisons between radar and aircraft shown in Figs. 1–5, referred to here as cases 1–5, respectively. The columns indicate temperature (T), aircraft-measured median volumetric diameter (D_0), radar-measured reflectivity factor minus the aircraft-inferred value (ΔZ), and the change in particle mass given by (5) that would be necessary to bring the aircraft into agreement with the radar, on average (Δm). The D_0 and ΔZ columns contain the mean and standard deviation. Note that case 3 was different from the others in that it is of significantly mixed phase.

Case	T (°C)	D_0 (mm)	ΔZ (dB)	Δm
1	−31.9	0.27 ± 0.04	−0.74 ± 2.00	−8%
2	−14.5	1.91 ± 1.37	−1.04 ± 2.83	−11%
3	−6.9	1.89 ± 1.20	+9.11 ± 7.15	+185%
4	−20.9	0.75 ± 0.23	+0.26 ± 2.42	+3%
5	−9.8	1.64 ± 0.42	+0.32 ± 2.01	+4%

and Poisson sampling noise in the aircraft data resulting from the large particles (that are important for Z) being present at low concentrations.

In Figs. 2, 4 and 5, normal constant-speed scans were employed, and so the collocation between aircraft and radar was poorer. In case 2 from 20 October of the CLARE'98 campaign, the lateral displacement of the aircraft from the radar azimuth was no more than 500 m, but the temporal difference of up to 7 min meant that samples had to be translated up to 8 km (using the winds measured by the aircraft) along the 260° azimuth from Chilbolton before they could be compared, with the necessary assumption of no significant evolution (or sedimentation) during this time. The wind at the heights of these runs was 17–20 m s^{-1} toward Chilbolton and was fortuitously within 5° of the azimuth along which the aircraft was flying. In cases 4 and 5 from the CWVC project, the lateral displacements were up to 1.5 km, and the temporal differences of 4 and 6 min, respectively, meant that similar displacements had to be applied. The wind speeds on these 2 days were also of a similar magnitude, but 55° and 25° (respectively) from the 259° azimuth along which the aircraft was flying and the radar was scanning.

Despite the difficulties in exactly matching up the aircraft and radar samples, the agreement for cases 2, 4, and 5 is good, with a mean difference in Z of 1 dB or less (see Table 1), despite the much larger particle sizes (D_0 of up to 1.9 mm) and higher reflectivities than in case 1. These scans provide support for the use of (5) for calculating Rayleigh radar reflectivity over a wide range of particle size, ice water content, and reflectivity factor.

Figure 3 shows much poorer agreement than the other four cases, with the aircraft apparently underpredicting Z by on average 9.11 dB, indicating that the particle masses (or densities) should be greater by al-

most a factor of 3. This cloud was studied in detail by Hogan et al. (2003) who found it to be of mixed phase, with liquid water content up to 0.2 g m^{-3}. They reported the presence of high-density "sector plates" that grow only in the presence of the high ice supersaturations that occur when liquid water is present; these would explain the large discrepancy in reflectivity. Any riming induced by the presence of liquid water would also have increased particle density above that predicted by (5), although note that the liquid water was in the form of sub-20-μm droplets and so would not itself have contributed noticeably to Z. Significant liquid was not detected in the other runs.

Hence, the comparisons of this section support the use of (5) in calculating Rayleigh-scattering radar reflectivity values in ice clouds from aircraft, even at the large particle sizes to which the radar is sensitive, but the occurrence of supercooled water can lead to a substantial bias because of a tendency toward denser ice particles. The accuracy of aircraft-derived radar reflectivity values outside the Rayleigh-scattering regime is more questionable because of the uncertainty in the calculation of γ in (2). Matrosov et al. (2002) showed reasonable agreement between direct measurements by a vertically pointing 35-GHz radar and Z calculated from an aircraft in a spiral descent over the instrument. They used the Brown and Francis (1995) mass–size relationship and Mie scattering with spheres of diameter equal to the maximum dimension, although the range of Z was only from -20 to -15 dBZ. They also tested a relationship from Liu and Illingworth (2000) relating mass to equivalent-area diameter D_a and got much worse agreement. It should be mentioned that this is not evidence in itself that D_a is unsuitable to use in Mie calculations, because they used maximum dimension rather than D_a in the relationship, thereby substantially increasing the inferred mass of each particle, and hence Z. In practice, the deviation of 35-GHz scattering from the Rayleigh approximation is very small in ice clouds, and so we must await rigorous comparisons of 94-GHz radar measurements with in situ aircraft sampling before we can be fully confident that non-Rayleigh scattering is being accounted for accurately in the analysis of aircraft data.

4. The IWC(Z, T) relationship implicit in the Met Office model parameterization

Before proceeding to derive expressions relating radar reflectivity and temperature to IWC, it is illuminating to examine the relationship that arises from the assumptions made in the microphysical parameterization scheme of the Met Office model, as described by Wilson and Ballard (1999). The model assumes the ice particle size distribution to be of inverse-exponential form:

$$n(D) = N_0 \exp(-3.67D/D_0), \tag{8}$$

where D_0 is the median volumetric diameter and the number concentration "intercept parameter" N_0 (m^{-4}) has a dependence on temperature T (°C) given by

$$N_0 = 2 \times 10^6 \exp(-0.122T), \tag{9}$$

an expression that originates from data presented by Houze et al. (1979) and reproduced in the review of Ryan (1996). The reduction of N_0 with increasing temperature can be considered an implicit way of parameterizing aggregation and the dependence of ice nucleus concentration on temperatures. It should be stressed that this does not necessarily imply that *total* ice particle number concentration is a function of temperature; indeed, Field et al. (2005) recently reported no significant temperature dependence of the concentration of particles larger than 100 μm but found that the "normalized" intercept parameter of Testud et al. (2001) (a generalized version of N_0 for nonexponential distributions) decreased by two orders of magnitude between $-50°$ and 0°C.

Ice particle mass in the model is defined by

$$m(D) = aD^b, \tag{10}$$

where $a = 0.069$ kg m^{-2} and $b = 2$. For millimeter-sized particles this is larger than the Brown and Francis (1995) relationship in (5) by around a factor of 2 and so is not consistent with the findings of the previous section. However, the exponent of 2 is close to the value of 1.9 in (5) and is supported on theoretical grounds by consideration of the aggregation process (Westbrook et al. 2004).

From (8) and (10), ice water content is given by

$$\mathrm{IWC} = \int_0^\infty n(D)m(D)\,dD = 2aN_0(D_0/3.67)^3. \tag{11}$$

In a similar way, radar reflectivity factor Z (m^3) in the Rayleigh-scattering regime may be derived from (2) in Système Internationale (SI) units:

$$\begin{aligned} Z &= \frac{|K_i|^2}{0.93}\left(\frac{6}{\pi\rho_i}\right)^2 \int_0^\infty n(D)m(D)^2\,dD \\ &= 2.926 \times 10^{-8} a^2 N_0 D_0^5. \end{aligned} \tag{12}$$

We eliminate the unknown D_0 (m) from (11) and (12) to obtain IWC (kg m^{-3}):

$$\mathrm{IWC} = 1341 a^{-0.2} N_0^{0.4} Z^{0.6}. \tag{13}$$

It can be seen immediately from the low power of a that the IWC retrieved from Z is relatively insensitive to the

mass–size (or density) assumption; a halving of mass used by the model to close to the Brown and Francis (1995) value would result in retrieved IWC increasing by only 15% for a given measured Z. Some authors (e.g., Heymsfield et al. 2002) argue that the mass should be even lower, but again the effect on retrieved IWC would be small. Even the 185% increase in ice mass implied by the radar–aircraft comparisons in case 3 of the previous section (probably because of liquid water being present) would only correspond to a 19% reduction in the IWC inferred from a measurement of Z. Of course, this argument has considered only the dependence on a, but in the appendix it is shown that b has a similarly small effect.

Converting (13) to more conventional units for IWC (g m^{-3}) and Z (dBZ) and substituting in (9) and the Wilson and Ballard (1999) value of a results in

$$\log_{10} \mathrm{IWC} = 0.060Z - 0.0212T - 1.92, \qquad (14)$$

where T is in degrees Celsius. In section 6 this expression is used in parallel with an aircraft-derived relationship in the comparison of model and radar. In the appendix it is shown that, were we to have assumed D_0 rather than N_0 to be a function of temperature, we should expect IWC to be proportional to Z rather than to $Z^{0.6}$ at a constant temperature. Hence, in the analysis of aircraft data in the next section we will be able to distinguish the means by which temperature provides information on the size distribution.

We now investigate the effect of the unphysically large ice densities for $D < 143$ μm introduced in the Met Office model by using a single mass relationship as given by (10). Numerical integration reveals that for $D_0 < 300$ μm the values of Z and IWC are slightly below the values derived from (11) and (12). IWC is reduced by more than Z because it depends upon a lower moment, so that over the D_0 range 30–300 μm the slope of the exponent is 0.63 rather than 0.6. For a D_0 of 100 μm the value of IWC for a given Z is reduced by about one-half, but this corresponds to an IWC of only around 10^{-3} g m^{-3}, which is right at the low end of the observed and modeled PDFs in the comparisons of section 6.

5. Relationships derived from aircraft data

a. Rayleigh-scattering radar retrievals of the "expected value" of IWC and extinction coefficient

In deriving relationships from aircraft data, we first consider retrievals by a Rayleigh-scattering radar, that is, those with frequencies up to around 10 GHz. Figure 6a shows the individual values of IWC and 3-GHz reflectivity for each of the points in the EUCREX aircraft dataset. The large scatter indicates the error to be expected from a retrieval of IWC using Z alone. However, the temperature-dependent shading of each point indicates that additional knowledge of temperature T should greatly improve the retrieval of IWC (the shadings used are indicated by the legend in Fig. 6d, although it is not intended that individual values be read off). To derive the relationship IWC(Z, T), we first calculate regressions between IWC and Z in 5°C temperature intervals spanning the range of $-57.5° > T \geq -2.5$°C. These are actually derived by first computing the linear mean IWC in each 5-dB range of Z (and each 5°C temperature interval), followed by calculation of the least squares fit in logarithmic space. This intermediate step is important because direct fits in logarithmic space (e.g., Liu and Illingworth 2000) will tend to lead to the long-term linear mean IWC being underestimated by around 20%. The results are shown in Fig. 6b, with each regression only plotted in the 5th–95th percentile range of Z.

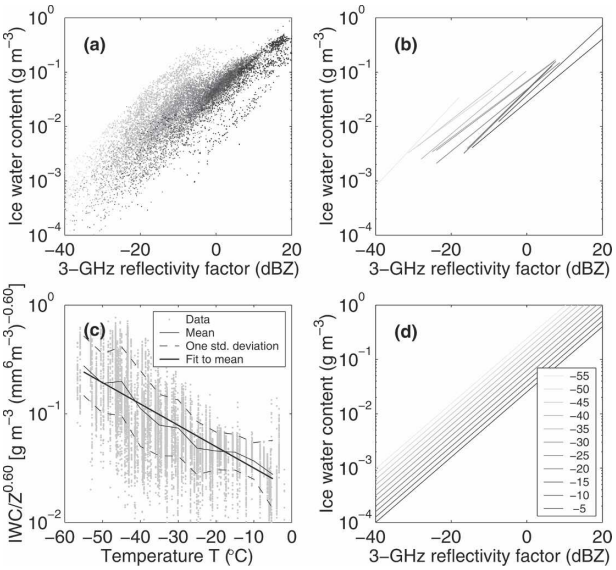

FIG. 6. Derivation of an empirical formula relating IWC to temperature and Z measured by a Rayleigh-scattering radar (e.g., at 3 GHz): (a) scatterplot of IWC vs Z from the EUCREX dataset, where the shading of each point indicates temperature [using the scale in (d)]; (b) IWC–Z regressions to the aircraft data in each 5°C temperature interval, plotting only the 5th–95th percentile of the Z data; (c) determination of the temperature-dependent term by calculating a least squares fit (thick solid line) to the mean values of IWC/$Z^{0.6}$ in each 5°C temperature interval (thin solid line); (d) the final relationship for IWC as a function of Z and temperature (°C).

So far our approach has been almost identical to Liu and Illingworth (2000), who then tabulated the regres-

sion coefficients for each of their fitted lines. It can be seen that the lines are almost parallel and show a clear temperature progression, with lower values of IWC for a given Z as T increases. However, it is easy to see how direct application of these different regression lines to real data can lead to discontinuities in the retrieved IWC field. We therefore hypothesize that the differences in slope and the fact that some of the lines cross are not robust features and that it is legitimate to seek a function that has a single power-law dependence on Z and varies smoothly with T. The mean slope of the regressions is 0.598, implying that the final function should have IWC proportional to $Z^{0.598}$. From the discussion in the appendix we note that this exponent is within the narrow 0.59–0.61 range that follows from the known spread of the mass–size exponent b, provided that temperature is taken to be a proxy for N_0. This therefore supports the contention that in midlatitude clouds the temperature dependence originates from N_0 and not D_0 as stated by Liu and Illingworth (2000). Given the uncertainty in the fitting of the power law, we conclude that the use of three significant figures is not justified here, and so we use an exponent of 0.60.

We next seek the functional dependence on temperature. If our relationship is to have IWC always proportional to $Z^{0.6}$, then IWC/$Z^{0.6}$ must be a function of T alone. Figure 6c shows all of the individual values of IWC/$Z^{0.6}$ plotted on a logarithmic scale against T. A linear mean of the points in each 5°C temperature interval (thin solid line) forms a nearly straight line, and a least squares fit (shown by the thick solid line in Fig. 6c) provides the coefficients c and d in the expression

$$\log_{10}(\mathrm{IWC}/Z^{0.6}) = cT + d. \tag{15}$$

Rearrangement then provides the final relationship, shown as the first formula in Table 2, where Z is given in conventional logarithmic units of reflectivity decibels (dBZ). Figure 6d shows the relationship plotted for the central temperature of the temperature ranges in which the original regressions (shown in Fig. 6b) were calculated. It is interesting that the formula is of the same form as (14) derived from the model assumptions, the only difference being the precise values of the coefficients. For the model to yield the same relationship as observed it would need to assume the Brown and Francis (1995) relationship rather than (10) and to replace (9) with $N_0 = (4.4 \times 10^6)\exp(-0.115T)$. This is actually closer than (9) to the observed spread of behavior reported by Ryan (1996).

We next apply the same procedure to obtain a relationship between visible extinction coefficient α and Rayleigh-scattering reflectivity. Regressions in 5°C temperature intervals indicate that on average $\alpha \propto Z^{0.52}$, and this time the exponent found directly from the data is retained. The result is the first formula in Table 3. Note that it is not valid to assume that particle cross-sectional area A is proportional to D_m^2 and hence that α should be proportional to $Z^{0.6}$ in the same way as IWC. Following the chain of argument in section 4, the exponent of 0.52 here implies that in fact $A \propto D_m^{1.6}$, which is consistent with the expressions of Mitchell (1996).

The instantaneous error in retrievals using these relationships may be estimated from the scatter of data in Fig. 6c and in the equivalent plot for the $\alpha(Z, T)$ formula (not shown). The dashed lines in Fig. 6c indicate that between −20° and −10°C, the rms error in retrieved IWC is around +50%/−33%, but for $T <$ −40°C it rises to +100%/−50%. This error is around the same as that found by Brown et al. (1995) when no size or temperature information was included, but it is pointed out that they did not make any correction for

TABLE 2. Formulas for deriving IWC (g m^{-3}) from radar reflectivity factor Z (dBZ) and temperature (°C) for three different radar frequencies. Two sets of equations are provided: the first for obtaining the expected value of IWC from a given Z and T and the second for ensuring that, when applied to a number of measured values, the inferred variance and PDF of IWC is unbiased. The radar calibration convention is described in section 2c.

Frequency (GHz)	Ice water content formula
Expected value	
3	$\log_{10}(\mathrm{IWC}) = 0.060Z - 0.0197T - 1.70$
35	$\log_{10}(\mathrm{IWC}) = (0.000\,242)ZT + 0.0699Z - 0.0186T - 1.63$
94	$\log_{10}(\mathrm{IWC}) = (0.000\,580)ZT + 0.0923Z - (0.007\,06)T - 0.992$
Unbiased variance	
3	$\log_{10}(\mathrm{IWC}) = 0.067Z - 0.0236T - 1.80$
35	$\log_{10}(\mathrm{IWC}) = 0.072Z - 0.0233T - 1.70$
94	$\log_{10}(\mathrm{IWC}) = 0.085Z - 0.0189T - 1.19$

TABLE 3. As in Table 2, but for retrievals of visible extinction coefficient α (m^{-1}) rather than IWC.

Frequency (GHz)	Visible extinction coefficient formula
Expected value	
3	$\log_{10}(\alpha) = 0.052Z - 0.0205T - 3.20$
35	$\log_{10}(\alpha) = (0.000\,447)ZT + 0.0683Z - 0.0171T - 3.11$
94	$\log_{10}(\alpha) = (0.000\,876)ZT + 0.0928Z - (0.005\,13)T - 2.49$
Unbiased variance	
3	$\log_{10}(\alpha) = 0.065Z - 0.0276T - 3.37$
35	$\log_{10}(\alpha) = 0.071Z - 0.0279T - 3.26$
94	$\log_{10}(\alpha) = 0.083Z - 0.0229T - 2.77$

the undercounting of small particles, which increases the scatter of the data. Some of the scatter could be due to the small sample volume of the aircraft probes, leading to statistical sampling noise in the dataset. An additional uncertainty arises because of fluctuations in the mass–size relationship, but it was shown in section 4 that a factor-of-2 error in mass (at all sizes) should lead to only a 15% error in retrieved IWC. The error in retrieved α is similar to that for IWC between $-20°$ and $-10°$C but rises to $+160\%/-62\%$ for $T < -40°$C. A larger error would generally be expected for α because it is one moment of the size distribution farther from Z than is IWC.

An additional source of error originates from the small-particle correction described in section 2b, which had a substantial effect on α. If the effect of the correction on α was wrong by a factor of 2 then this would result in the errors in the α retrievals increasing to $+60\%/-40\%$ between $-20°$ and $-10°$C, and $+220\%/-70\%$ for $T < -40°$C. The effect on the error of the IWC retrievals is much less.

b. *Non-Rayleigh-scattering radar retrievals of the expected value of IWC and extinction coefficient*

At high frequencies the large particles scatter outside the Rayleigh regime, reducing Z below that predicted by Rayleigh theory by in excess of 10 dB in some cases. This situation is demonstrated in Figs. 7a and 7b, which show the same parameters as Figs. 6a and 6b, but for 94 GHz rather than for 3 GHz. Although the regression line for $-55°$C is virtually the same, the lines for the warmer temperatures have steepened significantly. It is therefore no longer valid to assume a constant exponent in the power-law dependence of IWC on Z as before; we must incorporate its temperature dependence. This is achieved by first evaluating the IWC predicted by each of the regressions in Fig. 7b for two values of reflectivity factor: -20 and 0 dBZ. These are shown by the solid lines in Fig. 7c as a function of temperature. Both display an approximately linear relationship between temperature and the logarithm of IWC, although perhaps with outliers in the warmest and coldest bins. By fitting regressions to these two lines (shown by the dashed lines in Fig. 7c) and manipulating the regression coefficients, we derive an expression of a similar form to before, but with an extra term in which Z is multiplied by T. The second and third expressions in Table 2 show these expressions calculated for 35- and 94-GHz radars, respectively. The 94-GHz expression is plotted in Fig. 7d. It is important to note that the final expression is totally independent of which two reflectivity values were chosen to evaluate the regressions in Fig. 7c.

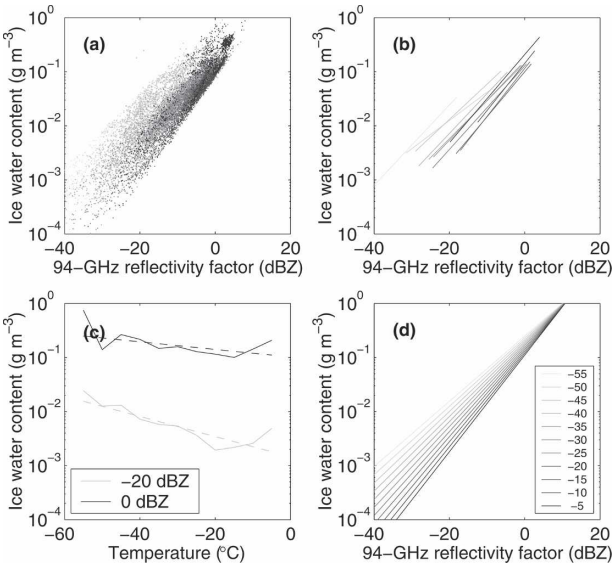

FIG. 7. Derivation of an empirical formula relating IWC to temperature and Z measured by a 94-GHz radar: (a) scatterplot of IWC vs Z from the EUCREX dataset, where the shading of each point indicates temperature [using the scale in (d)]; (b) IWC–Z regressions to the aircraft data in each 5°C temperature interval, plotting only the 5th–95th percentile of the Z data; (c) values of IWC according to the regressions in (b) at two values of Z vs temperature (solid lines), together with least squares fits (dashed lines); (d) the final relationship for IWC as a function of Z and temperature (°C).

The same procedure was applied with visible extinction coefficient α, as demonstrated at 35 GHz in Fig. 8, and the corresponding relationships are shown by the second and third formulas in Table 3.

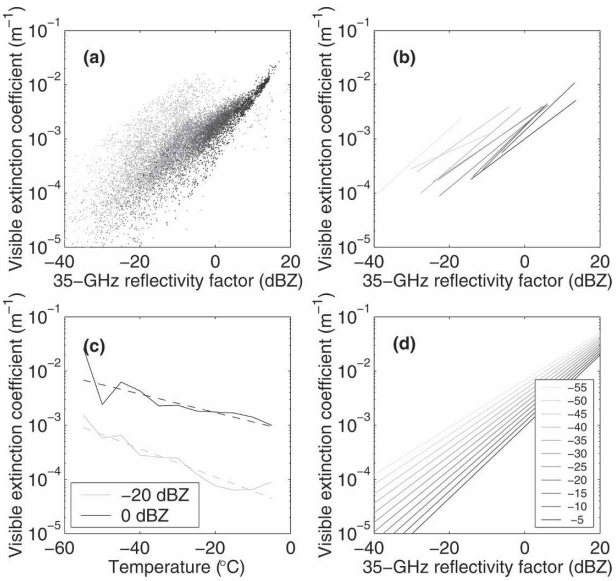

FIG. 8. As in Fig. 7, but for the retrieval of visible extinction coefficient using 35-GHz radar.

The errors were estimated by comparing the actual IWC and α with the values obtained from Z using the derived expressions. The fractional error of IWC from 35-GHz radar was +40%/−30% between −20° and −10°C, rising to +100%/−50% for $T < -40$°C. At 94 GHz the corresponding values were +55%/−35% and +90%/−47%. The fractional errors of α were about the same between −20° and −10°C, but for $T < -40$°C were higher: +170%/−63% at 35 GHz and +145%/−59% at 94 GHz.

These errors in the α–Z relationship are large, as is to be expected from the different moments involved, but it could still be useful as the first guess in an iterative multisensor algorithm. Nonetheless, support is provided by Matrosov et al. (2003), who analyzed 35-GHz radar profiles of ice clouds obtained in the Surface Heat Budget of the Arctic (SHEBA) experiment to estimate D_0 from the 20-min mean Doppler velocity, which they then combined with Z to derive α. Comparisons of the cloud optical depths, obtained by integrating the α profiles, with the more direct and independent estimate from the Atmospheric Emitted Radiance Interferometer (AERI) radiometer, indicated an uncertainty of about 77% in the radar technique. Matrosov et al. (2003) did not analyze their data in terms of temperature, but for their radar dataset they obtained the mean relationship

$$\log_{10} \alpha = 0.058Z - 2.4, \tag{16}$$

where α is in inverse meters and Z is in reflectivity decibels. They warned that this estimate is not robust but suggested it could be useful when only Z is available. It is remarkable that their equation is within 25% of the relationship in Table 3 for −35°C over the range from −40 to −10 dBZ; −35°C is a reasonable temperature for their Arctic ice clouds. Sassen and Liao (1995) also report α–Z relations, but they assumed either solid ice or ice–air mixtures with a density of 0.5 g m^{-3}; such unrealistically high densities lead to retrievals of α that are up to an order of magnitude lower than in Table 3.

c. *Relationships suitable for retrieval of the "unbiased variance" of IWC and α from radar*

The relationships derived so far are suitable for retrieving the best estimate of IWC or α for any given value of Z, but for some studies [such as those investigating the effects of cloud inhomogeneity on radiative transfer: e.g., Pomroy and Illingworth (2000) or Hogan and Kew (2005)], it is the horizontal variance or PDF of IWC or α that is required. Hogan and Illingworth (2003) showed that horizontal samples of IWC can often be reasonably well represented by a lognormal distribution; thus, a suitable parameter to characterize the width of the distribution would be $\sigma_{\ln\mathrm{IWC}}$, the standard deviation of lnIWC. This quantity is approximately equal to the fractional standard deviation $\sigma_{\mathrm{IWC}}/\mathrm{IWC}$. When a power-law expression is used to estimate $\sigma_{\ln\mathrm{IWC}}$ from a horizontal sample of Z, we are essentially obtaining it from $\sigma_{\ln Z}$, the standard deviation of ln$Z$. It is therefore essential for the power law to have a slope of $\sigma_{\ln\mathrm{IWC}}/\sigma_{\ln Z}$ in log–log space. However, it was pointed out by Hogan and Illingworth (2003) that a standard least squares fit in log–log space (as used in the previous sections) will yield a slope of $r\sigma_{\ln\mathrm{IWC}}/\sigma_{\ln Z}$, where r is the correlation coefficient between lnIWC and ln$Z$. Because r is invariably less than unity, $\sigma_{\ln\mathrm{IWC}}$ will tend to be underestimated by such a relationship.

Hogan and Illingworth (2003) therefore used the "standard deviation line" (hereinafter SD line), which by definition in this case has a slope of $\sigma_{\ln\mathrm{IWC}}/\sigma_{\ln Z}$ and passes through the point $(\overline{\ln\mathrm{IWC}}, \overline{\ln Z})$. However, they did not choose to include a temperature dependence, with the result that the mean IWC could be biased at particularly high or low temperatures, even though the retrieved fractional variance should be unbiased. They also only considered 94 GHz. We are therefore motivated to use their approach to derive a separate set of relationships for the express purpose of retrieving unbiased variances and PDFs but with suitable modification to allow reasonable estimates of the horizontal mean IWC or α to be retrieved as well.

Because it is generally the *horizontal* variance that is of interest, each of the 115 horizontal runs of the EUCREX dataset is considered separately. Figure 9b shows the SD lines relating IWC to 35-GHz reflectivity factor for each run, with the shading indicating the run-mean temperature. The length of each line indicates ±1 standard deviation. It should be noted that the temperature dependence of the slope of the SD line is much less significant than the temperature dependence of the slope of the least squares fit line, even at 94 GHz, and so we do not attempt to represent varying slope at any radar frequency. The mean slope in Fig. 9b is 0.72. To determine the temperature dependence of the relationship we follow a similar procedure to that of section 5a. For each run the mean IWC and Z are calculated in logarithmic space (i.e., the midpoints of the lines in Fig. 9b), and Fig. 9c shows the corresponding values of IWC/$Z^{0.72}$ plotted versus temperature. As before, the coefficients of the regression to these points (shown by the solid line) allow the full expression to be derived. Figure 9d shows the final relationship for IWC as a function of Z and T. This procedure is repeated for α and for all three frequencies, and the resulting expressions are shown in the lower halves of Tables 2 and 3.

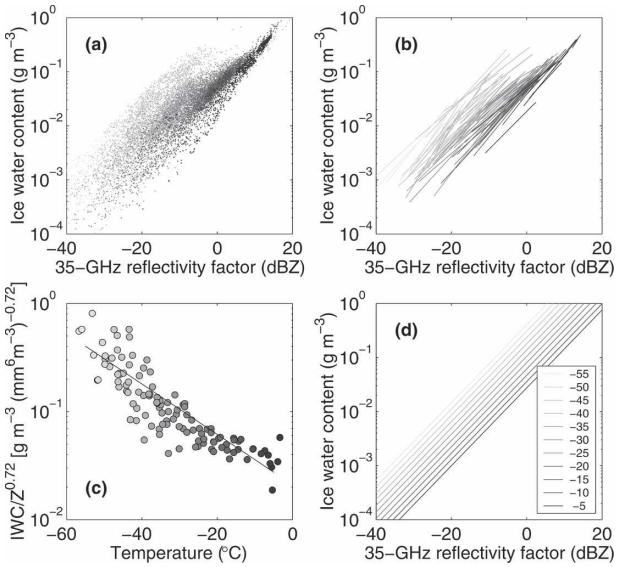

FIG. 9. Derivation of an empirical formula relating IWC to temperature and 35-GHz Z to be used for the retrieval of accurate variances and PDFs: (a) scatterplot of IWC vs Z from the EUCREX dataset, where the shading of each point indicates temperature [using the scale in (d)]; (b) SD lines fitted to the data from each of the 115 horizontal aircraft with their length indicating ±1 std dev; (c) IWC/$Z^{0.72}$ for the midpoints of each of the SD lines in (b) vs temperature (circles), with regression line; (d) the final relationships for IWC as a function of Z and temperature (°C).

The error in the retrieved fractional standard deviations of IWC and α may be estimated simply as the fractional standard deviation of the slopes of the SD lines for all EUCREX runs. In the case of $\sigma_{\ln\mathrm{IWC}}$, the rms errors are 24%, 21%, and 19% at 3, 35, and 94 GHz, respectively. For $\sigma_{\ln\alpha}$, the corresponding errors are 31%, 27%, and 23%.

6. Evaluation of the ice water content in precipitating clouds held in the Met Office mesoscale model

In this section, IWC retrieved using expressions in Table 2 is used to evaluate the values in the mesoscale version of the Met Office Unified Model. In addition, we apply the expression derived from the assumptions made in the model itself, as given by (14). The use of scanning 3-GHz radar has four distinct advantages over vertically pointing high-frequency cloud radars: First, the fact that the scattering is in the Rayleigh regime makes the returned signal much easier to interpret because $\gamma = 1$ in (2). Second, the very low attenuation means that quantitative retrievals are possible in the ice above melting ice and rain, which is crucial to evaluating the performance of model clouds for their role in the hydrological cycle. Third, radar calibration is accurate to 0.5 dB using the polarimetric technique of Goddard et al. (1994), as compared with 1–2 dB for most cloud radars. Last, the scanning capability allows a more representative sample of the clouds in a model grid box to be built up.

The Chilbolton 3-GHz radar does not operate continuously, and so we restrict the analysis to precipitating clouds observed over a total of 39 h spanning eight frontal events between August and December of 2000. Vertical scans with 300-m horizontal resolution were used, sampling at 0.1°–0.2° elevation steps from 0° to 30°. The scan sequence usually consisted of a full circle of scans 15° apart in azimuth, although on some days a sequence sampling only one quadrant was employed. Ice water content was derived from radar reflectivity and model temperature and was averaged horizontally to 12 km to correspond to the horizontal model spacing. In height, averages were calculated to correspond to the vertical model level spacing (around 500 m in the midtroposphere). Only measurements with surface rainfall directly beneath them were used, as indicated by Z in the lowest elevation ray being greater than 12 dBZ (corresponding to a rain rate of around 0.2 mm h^{-1}). For pixels above rain with no signal detected, IWC was taken to be zero. Because of the reduction of sensitivity with range, only data out to 36 km (equivalent to three model grid boxes) were used. The minimum detectable reflectivity for a 300-m/0.25-s sample is around −22 dBZ at 10 km and −11 dBZ at 36 km. From the first expression in Table 2, at −10°C these values translate to minimum detectable ice water contents of 0.0015 and 0.0069 g m^{-3}, respectively, rising to 0.009 and 0.042 g m^{-3} at −50°C. In the analysis of the results, the effect of this limitation is examined.

Hourly three-dimensional model forecast fields were used, consisting of a concatenation of the 6–11-h forecast from each of the four daily operational forecasts, the shorter-range forecasts being affected by spinup effects. The horizontal spacing of the model is around 12 km over the United Kingdom, and there are 35 levels in the vertical direction [see Cullen (1993) for details]. For comparison of means and PDFs with the radar, 15 × 15 model boxes were used, except when the radar was concentrating on one quadrant, when only 8 × 8 boxes were used. Only model columns associated with nonzero surface rainfall were considered.

Figure 10 shows a comparison of mean modeled and retrieved IWC in precipitating events over all eight cases, plotted against the temperature held in the model. The thin dot–dashed and dotted lines indicate the minimum detectable instantaneous values of IWC

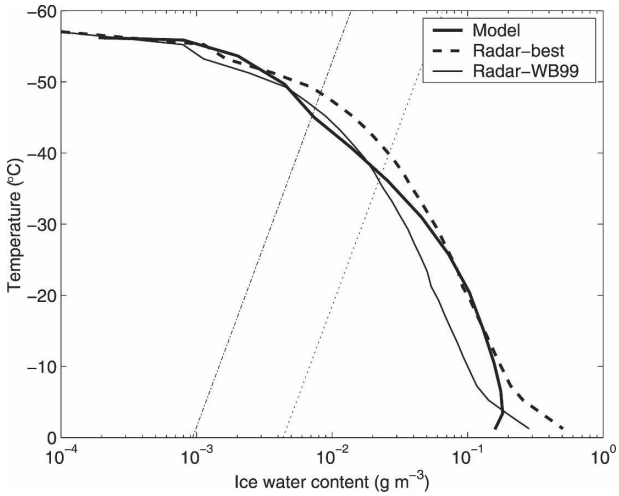

FIG. 10. Profiles of mean IWC over the eight cases from the model and the radar. The best radar retrieval uses the first expression in Table 2, and "WB99" uses the Wilson and Ballard (1999) expression given by (14). The thin dot–dashed line indicates the minimum detectable IWC at 10 km from the radar, and the dotted line is the corresponding value at 36 km.

at ranges of 10 and 36 km from the radar, respectively. We consider first the comparison with the "best" retrieval using the equation derived from aircraft data (the first in Table 2), as shown by the thick dashed line. It can be seen that the agreement between −30° and −10°C is extremely good. In this region the standard error on the mean is likely to be no more than around 25%; the error of instantaneous retrievals (indicated by the scatter in Fig. 6) will be largely averaged out over the eight cases considered, which are a similar sample and of the same types of cloud as the EUCREX dataset. Also, as illustrated in section 4, the relationship is relatively resilient to the increased mass of particles that may have been present if any of the cases were significantly mixed phase.

At warmer temperatures the thick lines in Fig. 10 begin to diverge, which could be due to accelerated aggregation in this temperature range (e.g., Pruppacher and Klett 1997) that is not represented in the model or possibly ontamination of the radar data by the enhanced return from the melting layer. At temperatures colder than −30°C the lines also diverge, with an apparent underestimate by the model of around a factor of 2 at −45°C. Although these mean IWC values are close to the instantaneous sensitivity of the radar, the finding of an underestimate by the model is robust because the effect of tenuous clouds not being detected can only be to reduce the radar-retrieved mean IWC. At temperatures colder than −50°C the model and radar appear to converge again, although this finding is certainly not robust: the fact that mean IWC here is below the instantaneous radar sensitivity indicates that, as one would expect, most precipitation events at midlatitudes do not extend to up to the −50°C level, and this average is from the unreliably small sample of cases that do extend to very cold temperatures.

The mean IWC estimated from the radar using the relationship derived from the model assumptions (the thin solid line in Fig. 10) is around 35% less than the best radar estimate. As discussed in section 5a, this condition is due to the fact that N_0 is likely to be underpredicted by (9) and, to a lesser extent, the different mass–size relationship.

Figure 11 compares PDFs of IWC from the radar and the model. The radar values were calculated from the unbiased-variance expression of Table 2 and were averaged to the model gridbox size. This expression gives a more representative spread of values and so is more suited to comparison of PDFs than is the expected-value expression, as explained in section 5c. Nonetheless, it results in only a 10% increase in the spread of values relative to the spread for the expected-value expression, which is smaller than the difference when comparing the other lines in Fig. 11. It can be seen that the model has a tendency in all temperature ranges to underpredict the spread of IWC found in the observations, probably because of the natural tendency of numerical models to smooth out features at close to the grid scale. The effect is most pronounced between −15° and 0°C, in which range the model exhibits a distinct mode at 0.2 g m^{-3} and the distribution from the radar is much flatter. Between −45° and −30°C the distributions are in good agreement for IWC $<$ 0.05 g m^{-3}, although the model predicts IWC $>$ 0.1 g m^{-3} less frequently than is observed. Note that the comparison is somewhat questionable at low values of IWC because of the instantaneous radar sensitivity at these temperatures varying with range between around 0.003 and 0.03 g m^{-3}, although in practice the sensitivity will be somewhat higher for the 12-km averaging performed to match the model resolution. No comparison is shown for temperatures colder than −45°C because of the typical IWC values here being below the instantaneous radar sensitivity.

7. Conclusions

In this paper, relationships have been derived for ice water content as a function of radar reflectivity factor and temperature. Comparisons of radar and aircraft suggest that the Brown and Francis (1995) mass–size relationship is suitable for calculating Rayleigh-scattering reflectivity from aircraft over a wide range of

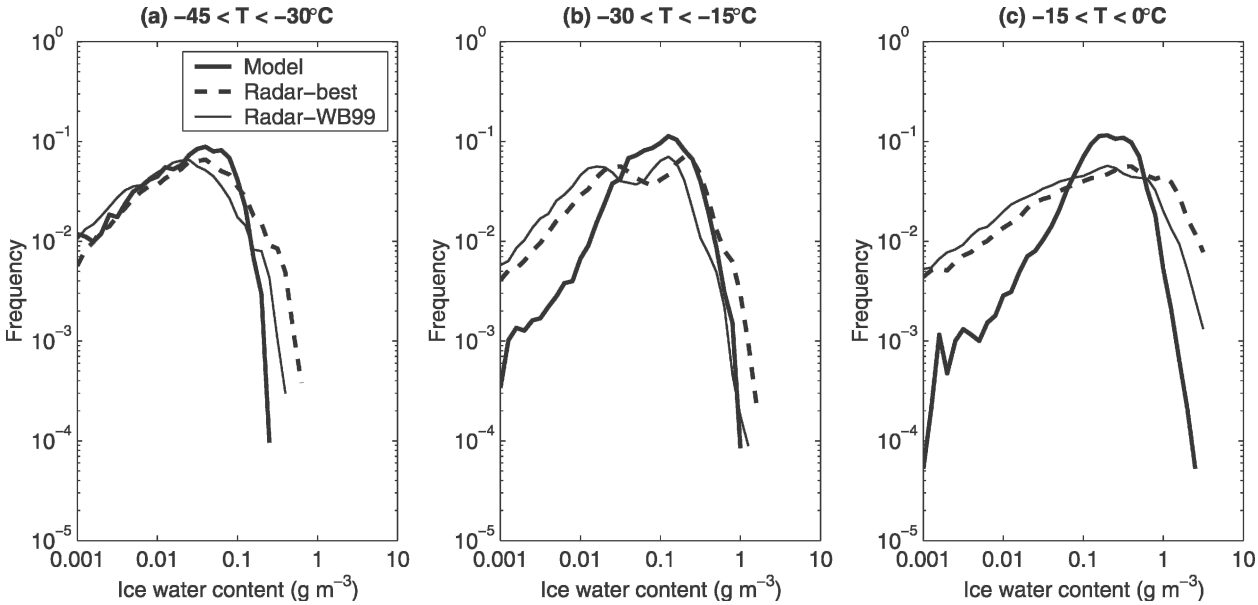

FIG. 11. Probability density functions of IWC in 15°C temperature ranges from both the model and the radar. The radar values have been averaged to the size of the model grid boxes and were derived using the 3-GHz unbiased-variance expression in Table 2 (labeled as best) and (14) (labeled as WB99).

particle size, ice water content, and radar reflectivity factor. The subsequent derivation of the relationships from a large midlatitude aircraft dataset extends the analysis of Liu and Illingworth (2000) in the following six important ways:

1) Single expressions were obtained that vary smoothly with temperature, solving the problem of 6°C discontinuities between the separate Liu and Illingworth (2000) relationships.
2) In addition to IWC, expressions for visible extinction coefficient have been derived. Extinction coefficient is the foremost parameter in determining the shortwave radiative properties of the cloud. Note that the errors in retrievals of this parameter are considerably higher than for IWC and are sensitive to the treatment of small particles in the aircraft analysis. These formulas therefore need careful testing before being used operationally.
3) A correction was performed to the aircraft size spectra to account for the undersampling of small crystals by the 2D-C probe, consistent with the magnitude of the bias found by McFarquhar and Heymsfield (1997).
4) Separate relationships have been obtained for estimating the expected value and the variance. As can be seen in Tables 2 and 3 [and as stressed by Hogan and Illingworth (2003)], there are substantial differences in slope, and thus it is important that the right one is used depending on the application.
5) Frequencies of 3 (i.e., Rayleigh scattering), 35, and 94 GHz have been considered.
6) The IWC–Z regressions were calculated in logarithmic space to the linear mean IWC in 5-dBZ bins of Z, thereby ensuring that the long-term linear mean of the retrieved IWC should be unbiased.

We find that, in Rayleigh-scattering conditions, plots of lnIWC versus ln$Z$ for a given temperature had a slope of 0.6 and for different temperatures the data lay on a series of parallel straight but horizontally displaced lines. As argued in the appendix, this result implies that the temperature dependence arises through N_0 rather than D_0.

The derived relationships are particularly suited to spaceborne radar retrievals (e.g., Stephens et al. 2002). Before they are applied globally, however, aircraft data from other geographical areas, in particular the Tropics where the relationships are unlikely to be the same, would have to be analyzed. The approach of using D_m as the diameter of a sphere for Mie calculations at 94 GHz has yet to be fully validated, but at lower frequencies this ambiguity disappears along with the problem of attenuation by liquid water and melting ice. This fact suggests that the higher elevation scans from operational weather radar could be useful for the assimilation of IWC into forecast models.

We have applied the retrieval technique to obtain IWC from 39 h of scanning 3-GHz radar data in precipitating clouds in the United Kingdom, and for the

first time we have been able to evaluate the values held in the operational mesoscale version of the Met Office forecast model. The mean IWC in the model was found to agree with the observations to within 10% at temperatures between −30° and −10°C, although it tended to underestimate IWC at colder temperatures.

Acknowledgments. The Chilbolton radar data were provided by the Rutherford Appleton Laboratory, and the model forecasts were provided by the Met Office and Peter Panagi. The EUCREX aircraft data were provided by Phil Brown. Darcy Ladd is thanked for implementing the aircraft-tracking variable-scan-speed capability of the Chilbolton radar. MPM acknowledges the Met Office for funding support. The CLARE'98 campaign was funded by the European Space Agency (Grant 12957/98). The CWVC experiment was funded by The UK Natural Environment Research Council under Grants NER/T/S/00105 and T/S/2000/01023.

APPENDIX

What is the Origin of the Temperature Dependence of the IWC–*Z* Relationship?

The explanation for the temperature dependence of the IWC–Z relationship that was found in section 5 can be split into two parts: 1) determining which variable of the size distribution is responsible for this temperature dependence and 2) understanding the physical processes that lead to this behavior in the size distribution. In this appendix we answer the first part and briefly speculate on the second part.

Ryan (1996) examined the findings from a number of aircraft campaigns worldwide and demonstrated that both N_0 and D_0 in (8) have a temperature dependence but also demonstrated that the functional relationship between N_0 and temperature is less systematic than for D_0 and that geographical variations are evident. Liu and Illingworth (2000) stated that the dependence of the IWC–Z relationship on temperature arose because of the temperature dependence of particle size (i.e., D_0), but this appears not to be the case.

We first test the hypothesis that it is the temperature dependence of N_0 that is important. We assume that, *at constant temperature,* N_0 is approximately constant (or, in specific terms, that it does not vary systematically with IWC) and hence that the relationship between Z and IWC arises entirely from variations in D_0. This assumption was made in section 4, and by eliminating D_0 from (11) and (12) it was found that IWC $\propto Z^{0.6}$ for constant temperature, a Rayleigh-scattering radar, and $b = 2$. In reality b can vary, which changes (13) to

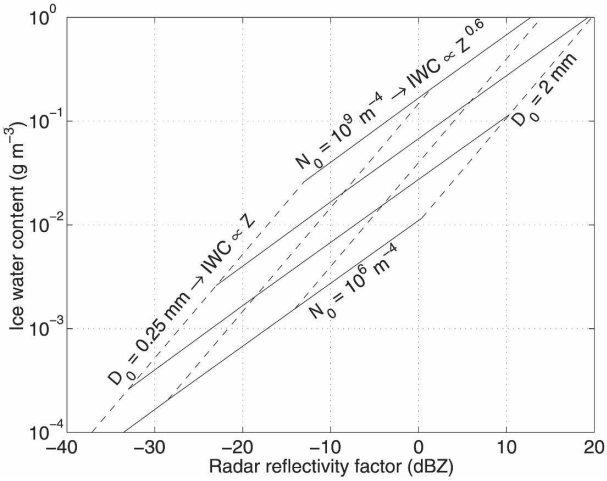

FIG. A1. Ice water content vs reflectivity factor for a Rayleigh-scattering radar for inverse-exponential distributions of the type given by (8) and the Brown and Francis (1995) mass–size relationship. The four solid lines are for distributions with constant number concentration parameters N_0 of 10^6, 10^7, 10^8, and 10^9 m^{-4}; the dashed lines are for distributions with constant median volume diameters D_0 of 0.25, 0.5, 1, and 2 mm. It can be seen that when N_0 is held fixed IWC is approximately proportional to $Z^{0.6}$ and that when D_0 is held fixed IWC is proportional to Z.

$$\mathrm{IWC} \propto N_0^{b/(2b+1)} Z^{(b+1)/(2b+1)}. \tag{A1}$$

Mitchell (1996) found that for common particle habits b ranges between 1.8 and 2.3; so we should find that for a given temperature the Z exponent lies in the narrow range of 0.59–0.61. This is indeed what was found in section 5 using real size distributions and implies that the temperature dependence arises through N_0 in (A1) because D_0 has been eliminated. This situation is illustrated in Fig. A1, which shows IWC versus Z for an inverse-exponential distribution with various values of N_0 and D_0. Comparison with Fig. 6b shows that the aircraft IWC–Z lines in each temperature range do indeed lie along constant N_0 rather than constant D_0 lines. We next test the alternative hypothesis that it is the temperature dependence of D_0 that is important by instead eliminating N_0 from the IWC and Z expressions [i.e., the variable-b versions of (11) and (12)] to obtain

$$\mathrm{IWC} \propto D_0^{-b} Z. \tag{A2}$$

Hence, if temperature dependence arises because temperature is a proxy for D_0 (or, in more specific terms, because at a given temperature D_0 does not vary systematically with IWC or Z), then we should expect IWC to be proportional to Z at constant temperature and the aircraft lines in Fig. 6b to be parallel to the dashed lines in Fig. A1. This is clearly not observed. Although the average value of D_0 certainly does have a

temperature dependence, the key point is that for constant temperature it still varies systematically with IWC and so its temperature dependence is not useful in refining the IWC–Z relationship. By contrast, methods exist in which extra information is invoked that is genuinely a proxy for particle size, such as the dual-wavelength ratio measured by two radars of different wavelengths; Hogan et al. (2000) showed that at constant dual-wavelength ratio IWC is proportional to Z. Atlas et al. (1995) similarly found a family of lines with unit gradient when they classified their Z and IWC data by mean size.

The reason for the relationship between N_0 and temperature is likely to be both the increase in the concentration of ice nuclei at colder temperatures and the fact that aggregation will act to reduce the number concentration of particles lower down into a cloud.

REFERENCES

Atlas, D., S. Y. Matrosov, A. J. Heymsfield, M.-D. Chou, and D. B. Wolff, 1995: Radar and radiation properties of ice clouds. *J. Appl. Meteor.,* **34,** 2329–2345.

Boudala, F. S., G. A. Isaac, Q. Fu, and S. G. Cober, 2002: Parameterization of effective ice particle size for high-latitude clouds. *Int. J. Climatol.,* **22,** 1267–1284.

Brown, P. R. A., and P. N. Francis, 1995: Improved measurements of the ice water content in cirrus using a total-water probe. *J. Atmos. Oceanic Technol.,* **12,** 410–414.

——, A. J. Illingworth, A. J. Heymsfield, G. M. McFarquhar, K. A. Browning, and M. Gosset, 1995: The role of spaceborne millimeter-wave radar in the global monitoring of ice-cloud. *J. Appl. Meteor.,* **34,** 2346–2366.

Carlin, B., Q. Fu, U. Lohmann, G. G. Mace, K. Sassen, and J. M. Comstock, 2002: High-cloud horizontal inhomogeneity and solar albedo bias. *J. Climate,* **15,** 2321–2339.

Cullen, M. J. P., 1993: The Unified Forecast/Climate Model. *Meteor. Mag.,* **122,** 81–94.

Donovan, D. P., M. Quante, I. Schlimme, and A. Macke, 2004: Use of equivalent spheres to model the relation between radar reflectivity and optical extinction of ice cloud particles. *Appl. Opt.,* **43,** 4929–4940.

European Space Agency, 1999: *CLARE'98 Cloud Lidar and Radar Experiment.* ESA/ESTEC, 239 pp.

Field, P. R., R. Wood, P. R. A. Brown, P. H. Kaye, E. Hirst, R. Greenaway, and J. A. Smith, 2003: Ice particle interarrival times measured with a fast FSSP. *J. Atmos. Oceanic Technol.,* **20,** 249–261.

——, R. J. Hogan, P. R. A. Brown, A. J. Illingworth, T. W. Choularton, P. H. Kaye, E. Hirst, and R. Greenaway, 2004: Simultaneous radar and aircraft observations of mixed-phase cloud at the 100-m-scale. *Quart. J. Roy. Meteor. Soc.,* **130,** 1877–1904.

——, ——, ——, ——, ——, and R. J. Cotton, 2005: Parameterization of ice particle size distributions for mid-latitude stratiform cloud. *Quart. J. Roy. Meteor. Soc.,* **131,** 1997–2017.

Francis, P. N., P. Hignett, and A. Macke, 1998: The retrieval of cirrus cloud properties from aircraft multi-spectral reflectance measurements during EUCREX'93. *Quart. J. Roy. Meteor. Soc.,* **124,** 1273–1291.

Fu, Q., B. Carlin, and G. G. Mace, 2000: Cirrus horizontal inhomogeneity and OLR bias. *Geophys. Res. Lett.,* **27,** 3341–3344.

Gardiner, B. A., and J. Hallett, 1985: Degradation of in cloud forward scattering spectrometer probe measurements in presence of ice particles. *J. Atmos. Oceanic Technol.,* **2,** 171–180.

Goddard, J. W. F., J. Tan, and M. Thurai, 1994: Technique for calibration of meteorological radars using differential phase. *Electron. Lett.,* **30,** 166–167.

Gultepe, I., G. A. Isaac, and S. G. Cober, 2001: Ice crystal number concentration versus temperature. *Int. J. Climatol.,* **21,** 1281–1302.

Heymsfield, A. J., and D. G. Baumgardner, 1985: Summary of workshop on processing 2-D probe data. *Bull. Amer. Meteor. Soc.,* **66,** 437–440.

——, S. Lewis, A. Bansemer, J. Iaquinta, L. M. Miloshevich, M. Kajikawa, C. Twohy, and M. Poellot, 2002: A general approach for deriving the properties of cirrus and stratiform ice cloud particles. *J. Atmos. Sci.,* **59,** 3–29.

Hogan, R. J., and A. J. Illingworth, 1999: The potential of spaceborne dual-wavelength radar to make global measurements of cirrus clouds. *J. Atmos. Oceanic Technol.,* **16,** 518–531.

——, and ——, 2003: Parameterizing ice cloud inhomogeneity and the overlap of inhomogeneities using cloud radar data. *J. Atmos. Sci.,* **60,** 756–767.

——, and S. F. Kew, 2005: A 3D stochastic cloud model for investigating the radiative properties of inhomogeneous cirrus clouds. *Quart. J. Roy. Meteor. Soc.,* **131,** 2585–2608.

——, A. J. Illingworth, and H. Sauvageot, 2000: Measuring crystal size in cirrus using 35- and 94-GHz radars. *J. Atmos. Oceanic Technol.,* **17,** 27–37.

——, P. N. Francis, H. Flentje, A. J. Illingworth, M. Quante, and J. Pelon, 2003: Characteristics of mixed-phase clouds—1. Lidar, radar and aircraft observations from CLARE'98. *Quart. J. Roy. Meteor. Soc.,* **129,** 2089–2116.

Houze, R. A., P. V. Hobbs, P. H. Herzegh, and D. B. Parsons, 1979: Size distributions of precipitation particles in frontal clouds. *J. Atmos. Sci.,* **36,** 156–162.

Liao, L., and K. Sassen, 1994: Investigation of relationships between K_α-band radar reflectivity and ice and liquid water content. *Atmos. Res.,* **34,** 299–313.

Liou, K.-N., 1986: Influence of cirrus clouds on weather and climate processes: A global perspective. *Mon. Wea. Rev.,* **114,** 1167–1199.

Liu, C.-L., and A. J. Illingworth, 2000: Toward more accurate retrievals of ice water content from radar measurement of clouds. *J. Appl. Meteor.,* **39,** 1130–1146.

Locatelli, J. D., and P. V. Hobbs, 1974: Fall speeds and masses of solid precipitation particles. *J. Geophys. Res.,* **79,** 2185–2197.

Mace, G. G., T. P. Ackerman, E. E. Clothiaux, and B. A. Albrecht, 1997: A study of composite cirrus morphology using data from a 94-GHz radar and correlations with temperature and large scale vertical motion. *J. Geophys. Res.,* **102,** 13 581–13 593.

Matrosov, S. Y., A. V. Korolev, and A. J. Heymsfield, 2002: Profiling cloud ice mass and particle characteristic size from Doppler radar measurements. *J. Atmos. Oceanic Technol.,* **19,** 1003–1018.

——, M. D. Shupe, A. J. Heymsfield, and P. Zuidema, 2003: Ice cloud optical thickness and extinction estimates from radar measurements. *J. Appl. Meteor.,* **42,** 1584–1597.

McFarquhar, G. M., and A. J. Heymsfield, 1997: Parameterization of tropical cirrus ice crystal size distributions and implications for radiative transfer: Results from CEPEX. *J. Atmos. Sci.,* **54,** 2187–2200.

Mitchell, D. L., 1996: Use of mass- and area-dimensional power laws for determining precipitation particle terminal velocities. *J. Atmos. Sci.,* **53,** 1710–1723.

Pomroy, H. R., and A. J. Illingworth, 2000: Ice cloud inhomogeneity: Quantifying bias in emissivity from radar observations. *Geophys. Res. Lett.,* **27,** 2101–2104.

Pruppacher, H. R., and J. D. Klett, 1997: *Microphysics of Clouds and Precipitation.* Kluwer, 954 pp.

Ryan, B. F., 1996: On the global variation of precipitating layer clouds. *Bull. Amer. Meteor. Soc.,* **77,** 53–70.

Sassen, K., and L. Liao, 1995: Estimation of cloud content by W-band radar. *J. Appl. Meteor.,* **35,** 932–938.

Stephens, G. L., and Coauthors, 2002: The CloudSat Mission and the A-Train. *Bull. Amer. Meteor. Soc.,* **83,** 1771–1790.

Strapp, J. W., F. Albers, A. Reuter, A. V. Korolev, U. Maixner, E. Rashke, and Z. Vukovic, 2001: Laboratory measurements of the response of a PMS OAP-2DC. *J. Atmos. Oceanic Technol.,* **18,** 1150–1170.

Testud, J., S. Oury, X. Dou, P. Ameyenc, and R. Black, 2001: The concept of normalized distribution to describe raindrop spectra: A tool for cloud physics and cloud remote sensing. *J. Appl. Meteor.,* **40,** 1118–1140.

Westbrook, C. D., R. C. Ball, P. R. Field, and A. J. Heymsfield, 2004: Universality in snowflake formation. *Geophys. Res. Lett.,* **31,** doi:10.1029/2004GL020363.

Wilson, D. R., and S. P. Ballard, 1999: A microphysically based precipitation scheme for the UK Meteorological Office Unified Model. *Quart. J. Roy. Meteor. Soc.,* **125,** 1607–1636.